DEVELOPMENT OF FRACTURE PLANES DURING CREEP IN GRANITE

David Lockner and James Byerlee

U. S. Geological Survey

Menlo Park, CA 94025

A cylindrical sample of Westerly Granite was subjected to a constant confining pressure of 500 bars and differential stress of 5100 bars. Acoustic emission (AE). axial strain and P wave velocity were monitored during the 60 hours preceding failure. AE and strain were closely correlated during primary, secondary, and tertiary creep phases of the experiment. Approximately 50,000 AE events were located from arrival time data during the experiment. These results show that during primary and secondary creep, AE events occurred randomly throughout the sample. The onset of tertiary creep, however, was accompanied by an abrupt concentration of AE events in a zone that was part of the eventual failure plane. This finding suggests that brittle fracture in granite is the culmination of an unstable process in which crack growth occurs in a localized region during tertiary creep.

Second Conference on Acoustic Emission/Microseismic Activity in Geologic Structures and Materials — The Pennsylvania State University, November 13–15, 1978.

INTRODUCTION

Understanding the process of brittle fracture in rock has been a long standing problem in rock mechanics. A key question that remains unanswered is how the stable small-scale cracking that occurs during transient (or primary) creep and during secondary creep changes material properties of the rock until an instability occurs, resulting in macroscopic failure. Another critical question, and one of practical application to earthquake prediction and other areas, involves the characterization of the transition from stable, homogeneous crack growth to unstable fracture.

The monitoring of acoustic emission during deformation of rock has been a useful tool in studying fracture mechanics. Mogi (1968) located microfractures in rock subjected to a bending moment and observed a localization of events on the fracture plane prior to failure. Scholz (1968a) studied the acoustic emission in granite under uniaxial loading and was able to locate acoustic emission events prior to shear failure. Lockner and Byerlee (1977a) reported three dimensional locations of microfractures during triaxial compression of granite and sandstone. In those experiments, we detected no significant localization of microfractures prior to failure, but owing to the nature of the experimental procedure, most of the microfractures recorded in the tests on granite occurred during the primary creep stage. This finding suggested that if localization of microfractures did occur, it must be in the late stages of creep, probably during tertiary creep. This hypothesis motivated the current

experiment in which acoustic emission was monitored during all three phases of creep at constant differential stress.

EXPERIMENTAL METHOD

A cylindrical sample of Westerly Granite, 7.63 cm in diameter and 19.05 cm in length, was loaded in a triaxial press to an axial stress of 5600 bars. A confining pressure of 500 bars was applied to the sample throughout the experiment. Six piezoelectric transducers, cemented to the sample, were used to monitor acoustic emission. An electronic timing system determined the relative arrival times at the six stations of each acoustic emission signal. Arrival times, measured to $\pm$ 0.05 μsec., were digitized and recorded on magnetic tape along with the peak amplitudes of the signals at each station. For a more detailed description of this system, see Byerlee and Lockner (1977). During the experiment, P-wave velocity was measured independently at angles of 23°, 36° and 90° to the axis of the sample to determine the velocity anisotropy. This was accomplished by successively pulsing source transducers with a pulse generator and measuring travel times to receiver transducers with a time delay oscilloscope. In addition, a strain gauge was used to measure axial strain.

The purpose of the experiment was to study acoustic emission during tertiary creep. Because the duration of the tertiary creep phase in Westerly Granite is highly sensitive to stress, it was impossible to know beforehand the exact differential stress at which

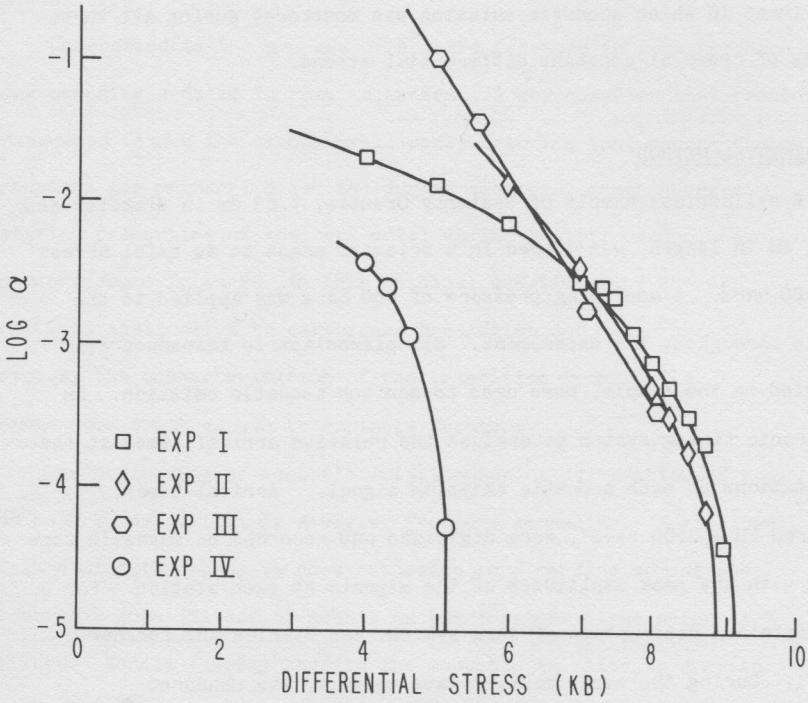

Figure 1. Plot of acoustic emission decay rate, α, during transient creep as a function of differential stress for four Westerly Granite samples. α is taken from $\log\left[\frac{dN}{dt}\right] = \beta - \alpha N$ where N is cumulative number of acoustic emission events. Exp I-III were at 1kb confining pressure. Exp IV was the experiment reported in this paper and was run at 500 bars confining pressure. Failure occurred where lines crossed horizontal axis. The data suggest that nearness to failure strength can be estimated from the slope of these curves.

the experiment should be run. The strategy we adopted was based on results of earlier acoustic emission experiments (Lockner and Byerlee, 1976). Differential stress was applied to the sample and the acoustic emission rate was monitored during transient creep. The rate of decay of acoustic emission (Fig. 1) was then used to estimate how close the sample was to its failure strength. In this way, differential stress was raised in steps to 5100 bars. The sample held this final stress level for 60 hours, advancing into a tertiary creep phase for the final 2.5 hours.

LOCATION METHOD

The technique used to locate microfractures from the acoustic emission arrival times, described earlier in Byerlee and Lockner (1977), estimates the event time, TE, and the three spatial coordinates, XE, YE, and ZE, for each acoustic emission event as well as the acoustic wave velocity, VE. First, an initial guess of the five parameters is made. Then, an adjustment vector, $dS = \left[d\,[TE], d\,[XE], d\,[YE], d\,[ZE], d\,[VE] \right]$ is calculated from a least squares fit of the arrival time data. The adjustments are then added to the initial estimates to give improved estimates of the five parameters. From these improved values, a new adjustment vector is calculated. This procedure is repeated until the parameters have converged on a best estimate. The adjustment vector is obtained by solving the equation

$$\begin{bmatrix} N & \Sigma CX & \Sigma CY & \Sigma CZ & \Sigma CV \\ \Sigma CX & \Sigma CX^2 & \Sigma CXCY & \Sigma CXCZ & \Sigma CXCV \\ \Sigma CY & \Sigma CXCY & \Sigma CY^2 & \Sigma CYCZ & \Sigma CYCV \\ \Sigma CZ & \Sigma CXCZ & \Sigma CYCZ & \Sigma CZ^2 & \Sigma CZCV \\ \Sigma CV & \Sigma CXCV & \Sigma CYCV & \Sigma CZCV & \Sigma CV^2 \end{bmatrix} \times \begin{bmatrix} d[TE] \\ d[XE] \\ d[YE] \\ d[ZE] \\ d[VE] \end{bmatrix} = \begin{bmatrix} \Sigma CR \\ \Sigma CRCX \\ \Sigma CRCY \\ \Sigma CRCZ \\ \Sigma CRCV \end{bmatrix} \qquad (1)$$

where

$$N = 6$$

$$CX = \frac{(XE - X_i)}{VE \cdot D_i}$$

$$CY = \frac{(YE - Y_i)}{VE \cdot D_i}$$

$$CZ = \frac{(ZE - Z_i)}{VE \cdot D_i}$$

$$CV = \frac{-D_i}{VE^2}$$

$$CR = t_i - \hat{t}_i$$

X_i, Y_i and Z_i are the coordinates of the i^{th} station, D_i the distance from the event to the i^{th} station, t_i the observed arrival time and $\hat{t}_i = TE + D_i/VE$.

The above procedure assumes an isotropic velocity field. In the experiment described in this paper, the differential stress was sufficient to produce a highly anisotropic velocity field, thereby violating a basic assumption of the location technique. To correct this, anisotropy terms were added to eq. (1), by redefining the constants to be:

$$N = 6$$

$$CZ = \gamma_i \frac{(ZE - Z_i)}{VE \cdot D_i}$$

$$CX = \frac{\gamma_i}{\zeta^2} \cdot \frac{(XE - X_i)}{VE \cdot D_i}$$

$$CV = \frac{1}{\gamma_i} \cdot \frac{-D_i}{VE^2}$$

$$CY = \frac{\gamma_i}{\zeta^2} \cdot \frac{(YE - Y_i)}{VE \cdot D_i}$$

$$CR = t_i - \hat{t}_i$$

with:

$$\gamma_i = \frac{\zeta}{\left[\cos^2\theta_i + \zeta^2 \sin^2\theta_i\right]^{1/2}}$$

$$\hat{t}_i = TE + \frac{D_i}{\gamma_i \cdot VE}$$

Because the sample and the stress field are radially symmetric, we assume the velocity field to be radially symmetric. Then, ζ is the ratio: radial velocity/axial velocity, γ_i is the ratio: velocity in direction of i^{th} station/axial velocity, and θ_i is the vertically projected angle to the i^{th} station. In this experiment, ζ was measured independently and supplied as a constant to the location program. VE is now an estimate of the axial velocity in the sample.

RESULTS

During the experiment, differential stress was raised in steps from 4000 bars to 5100 bars. We confine our discussion to the final part of the experiment, in which differential stress was held at 5100 bars for 60 hours before the sample failed catastrophically. During this time, approximately 50,000 acoustic emission events were recorded

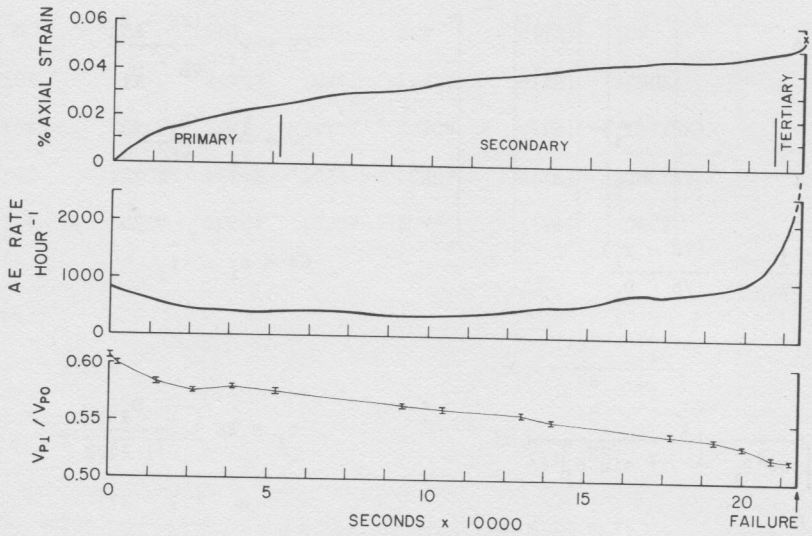

Figure 2. Plots of axial strain, acoustic emission rate and velocity prior to failure. Differential stress = 5100 bars was estimated to be between 85-90% of ultimate strength for this sample. Velocity plotted is the P-wave velocity measured perpendicular to the axis of the sample and normalized by hydrostatic P-wave velocity. Error bars indicate uncertainty due to reading errors of $\pm$ 0.03 μsec.

and located. Figure 2 shows axial strain and acoustic emission rate during this 60 hour period. The axial strain curve is divided into periods of primary, secondary and tertiary creep. The strain rate and acoustic emission rate are similar for primary and secondary creep but diverge markedly from each other during tertiary creep. These results are discussed in detail below. The compressional velocity measured perpendicular to the axis of the sample, $V_{p\perp}$, also plotted in Figure 2, is normalized by the P-wave velocity at hydrostatic stress at the beginning of the experiment. Note that the slope of the velocity curve is similar to the negative slope of the strain curve, even during tertiary creep.

Locations of the AE events recorded during the experiment are plotted in Figure 3. Event locations are divided into four groups: those occurring during primary creep, secondary creep, the first 8000 seconds of tertiary creep and the final 1100 seconds before failure. All four views show the projection of the events perpendicular to the eventual fracture plane. The fracture plane is shown on each plot for reference. Because of the large number of events, density maps are drawn in which contour units are number of events per square centimeter. The locations during primary and secondary creep form a diffuse pattern in the center of the sample. This pattern, commonly observed in similar experiments, indicates nearly uniform microfracturing. The number of events drops off near the sides of the sample because no correction is made for the smaller volume of rock represented by these regions of the plot. The absence of events near

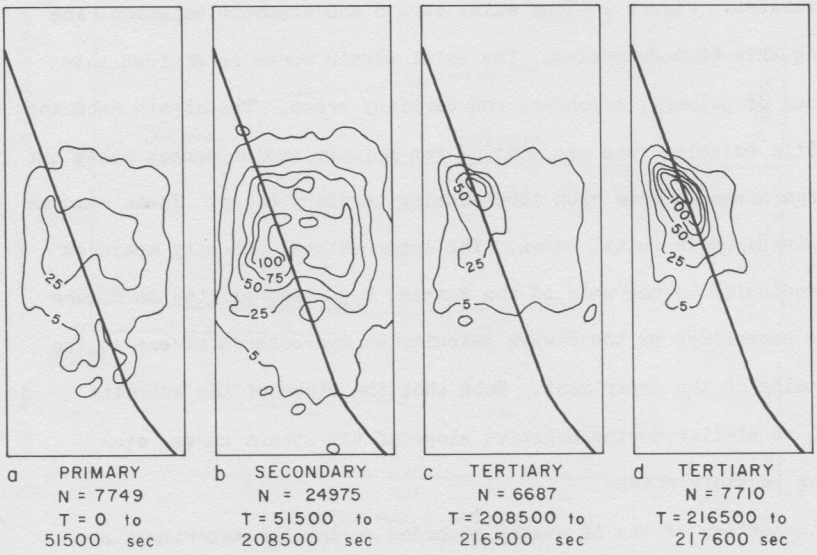

Figure 3. Concentration of AE events are plotted for periods of primary, secondary, and tertiary creep. Events occurring during teritary creep are divided into two groups, those occurring during the first 8000 seconds those occurring during the final 1100 seconds. Contour units are number of events/cm. All plots are viewed perpendicular to the eventual fracture plane. The trace of this plane is drawn in each figure for reference. Note nucleation of events on the eventual fracture plane coincides with onset of tertiary creep.

the ends of the sample has two primary causes. First, travel paths are much longer for events occurring near the ends of the sample than for those originating in the center. As a result, many events near the ends of the sample are lost through attenuation. Second, the ends of the sample are constrained by friction against the steel endplugs and therefore dilate less. In experiments of this type, we observe a close correlation between acoustic emission and strain. Since the ends of the sample are supported by the endplugs, the rate of emission should be lower from these regions than from the center of the sample.

The nearly uniform pattern occurring in the center of the sample changes in less than 5 minutes, at the onset of tertiary creep, to one in which the diffuse background pattern has superimposed on it a concentrated zone of cracking located directly on the eventual fracture plane (Fig. 3c). In the next 9000 seconds, this zone shows a marked increase in activity and apparently spreads along the fracture plane.

The term "tertiary creep" is used to describe the period in which strain rate increases, leading to macroscopic failure of the sample. If the tertiary creep phase in this experiment were taken from the strain record (Fig. 2) it would begin about 2000 seconds before failure. The sudden increase in acoustic emission rate prior to this time however suggests that, locally, tertiary creep began 9000 seconds before failure. This is also the time when the microfractures first began to concentrate. Because the acoustic emission rate appears more sensitive than the strain gauge reading, we take the onset of tertiary

creep to coincide with the localization of microfracturing, 9000 seconds before failure.

DISCUSSION

As the plots of Figure 2 shows, strain rate, acoustic emission rate, and rate of change of P wave velocity all behaved similarly during primary and secondary creep. This behavior can be explained if all these parameters are controlled by a single process, namely microcrack growth. Primary and secondary creep, phases of the experiment are characterized (Figure 3) by a random pattern of microfracturing in the central region of the sample.

During tertiary creep, a zone of intense cracking, about 2 cm in diameter, developed. The path of the acoustic wave used to measure $V_{p\perp}$ missed this zone by 2.7 cm. The strain gauge used to measure axial strain was 5.7 cm away, yet neither strain nor velocity showed measurable changes until about 2000 seconds before failure, whereas the acoustic emission rate began to increase 9000 seconds before failure. This finding agrees with the observation of AE sources showing that the first stages of the failure process were confined to a small volume of the sample (about 4 cc). Apparently, any anomalous changes in material properties that may have occurred were restricted to this small volume during the entire nucleation process observed. The nucleation center occurred 1 cm beneath the surface of the sample on the eventual fracture surface. Visual inspection of this region failed to reveal any inhomogeneity. Nucleation may have begun here in

response to the presence of the free surface, although there are not enough data to determine this.

In earlier experiments (Lockner and Byerlee, 1977a), we studied the failure process in both granite and sandstone. In those experiments, we observed no definite localization of microfractures prior to failure. However, the algorithm used to calculate those locations assumed an isotropic velocity. Because we had no direct measurements of velocity at that time, we could only assume an isotropic velocity. Now, with the additional information that (1) anisotropy can be large near failure, as was measured in this experiment and (2) localization of microfractures occur only during tertiary creep, we have taken a second look at one of the earlier experiments. We relocated events that occurred during tertiary creep in an experiment on Weber Sandstone assuming an anisotropy of $V_{p\perp}/V_p$ axial = 0.6. The improved locations obtained from the anisotropy model in that experiment showed a strong correlation with the fracture plane, a nucleus of intense cracking occurring directly on the fracture plane during tertiary creep.

CONCLUSIONS

One remarkable result of this experiment is that, for the first time, nucleation of the fracture plane in an intact, triaxially loaded sample was observed. It is satisfying that this nucleation coincided with the onset of tertiary creep. Primary and secondary creep were characterized by uniform, stable cracking in the sample. Unstable

tertiary creep apparently corresponded to inhomogeneous cracking that culminated in the rupture of the sample.

Another significant result is that velocity and strain measurements made within a few centimeters of the nucleation zone showed no change until well into the period of tertiary creep. This finding suggests that the first stages of failure can be expected to produce only local, and therefore hard to detect, changes in material properties.

REFERENCES

Byerlee, J. D. and D. A. Lockner, 1977, Acoustic emission during fluid injection in rock, Proceedings First Conference on Acoustic Emission/Microseismic Activity in Geologic Structures and Materials, Trans Tech Publications, Clausthal-Zellerfeld, W. Germany, p. 87-98.

Lockner D. A. and J. D. Byerlee, 1977a, Acoustic emission and fault location in rocks, Proceedings, First Conference on Acoustic Emission/Microseismic Activity in Geologic Structures and Materials, Trans. Tech. Publications, Clausthal-Zellerfeld, W. Germany, p. 99-107.

Lockner, D. A. and J. D. Byerlee, 1977b, Acoustic emission and creep in rock at high confining pressure and differential stress, Bul. Seism. Society Am., v. 67, no. 2, p. 247-248.

Mogi, K., 1968, Source location of elastic shocks in the fracturing process in rocks, Bull. Earthquake Research Institute, v. 46, p. 1103-1125.

Scholz, C. H., 1968a, Experimental study of the fracturing process in brittle rocks, Journal of Geophsyical Research, v. 73, p. 1447-1454.

Scholz, C. H., 1968b, The frequency-magnitude relation of micro-fracturing in rock and its relation to earthquakes, Bull. Seism. Soc. Am., v. 58, p. 399-415.